To appear in the Astrophysical Journal

AMMONIA IMAGING OF THE DISKS IN THE NGC 1333 IRAS 4A PROTOBINARY SYSTEM

MINHO CHOI[1], KEN'ICHI TATEMATSU[2], GEUMSOOK PARK[1,3], AND MIJU KANG[1,3]

ABSTRACT

The NGC 1333 IRAS 4A protobinary was observed in the ammonia (2, 2) and (3, 3) lines and in the 1.3 cm continuum with a high resolution (about 1.0″). The ammonia maps show two compact sources, one for each protostar, and they are probably protostellar accretion disks. The disk associated with IRAS 4A2 is seen nearly edge-on and shows an indication of rotation. The A2 disk is brighter in the ammonia lines but dimmer in the dust continuum than its sibling disk, with the ammonia-to-dust flux ratios different by about an order of magnitude. This difference suggests that the twin disks have surprisingly dissimilar characters, one gas-rich and the other dusty. The A2 disk may be unusually active or hot, as indicated by its association with water vapor masers. The existence of two very dissimilar disks in a binary system suggests that the formation process of multiple systems has a controlling agent lacking in the isolated star formation process and that stars belonging to a multiple system do not necessarily evolve in phase with each other.

Subject headings: accretion disks — binaries: general — ISM: individual (NGC 1333 IRAS 4A) — stars: formation

1. INTRODUCTION

The NGC 1333 region in Perseus is a site of active star formation producing a young cluster of Sun-like low-mass stars (Aspin et al. 1994; Bally et al. 1996; Rodríguez et al. 1999). IRAS 4A is one of the brightest submillimeter sources among the deeply embedded protostars in NGC 1333 (Sandell & Knee 2001). The cold spectrum of dust emission suggests that IRAS 4A is very young (Sandell et al. 1991), and IRAS 4A drives molecular outflows with an interesting morphology (Blake et al. 1995; Girart et al. 1999; Choi 2001). Radio interferometric observations revealed that there are two sources in IRAS 4A, probably gravitationally bound to each other (Lay et al. 1995; Looney et al. 2000).

In all the continuum images published so far, the primary, A1, is more luminous than the secondary, A2, by a factor of $\sim$3 (Looney et al. 2000; Reipurth et al. 2002; Girart et al. 2006), which suggests that A1 may be more massive than A2. However, recent observations in the SiO and the H_2 lines puzzlingly showed that the outflow driven by A2 (northeast-southwestern outflow) is much more powerful and larger than the one driven by A1 (southern outflow) (Choi 2005; Choi et al. 2006). This inverse relation between the (dust) mass and the outflow activity challenges conventional models of star formation since both of them are supposed to be positively correlated with the mass accretion rate (Cabrit & André 1991; Bachiller 1996).

To investigate the structure of the NGC 1333 IRAS 4A system, we observed the region in several molecular tracers. In this Letter, we present our high angular resolution observations in the NH_3 lines. In § 2 we describe our NH_3 observations. In § 3 we report the results of the NH_3 imaging and discuss the physical process in the IRAS 4A system.

2. OBSERVATIONS

The NGC 1333 IRAS 4 region was observed using the Very Large Array (VLA) of the National Radio Astronomy Observatory[4] in the NH_3 (2, 2) and (3, 3) lines (23722.6336 and 23870.1296 GHz, respectively) and in the λ = 1.3 cm continuum. Twenty-five antennas were used in the C-array configuration on 2004 March 5. The continuum was observed for 20 minutes at the beginning and for 10 minutes at the end of the observing track, and the NH_3 lines were observed for 5 hours in the midsection of the track. For each of the NH_3 lines, the spectral windows were set to have 64 channels with a channel width of 0.049 MHz, giving a velocity resolution of 0.62 km s^{-1}. For the 1.3 cm continuum, the observations were made in the standard K-band continuum mode (22.5 GHz or λ = 1.33 cm).

The phase tracking center was (α, δ) = ($03^{\rm h}29^{\rm m}10.41^{\rm s}$, 31°13′32.2″) in J2000.0. The nearby quasar 0336+323 (PKS 0333+321) was observed to determine the phase and to obtain the bandpass response. The flux was calibrated by observing the quasar 0713+438 (QSO B0710+439) and by setting its flux density to 0.49 Jy, which is the average of the flux density measured within a day of our observations (VLA Calibrator Flux Density Database[5]). Comparison of the amplitude gave a flux density of 1.97 Jy for 0336+323, and the flux uncertainty is $\sim$10%. To avoid the degradation of sensitivity owing to pointing errors, pointing was referenced by observing the calibrators at the X-band (3.6 cm). This referenced pointing was performed about once an hour and just before observing the flux calibrator.

Maps were made using a CLEAN algorithm. The NH_3 data produced synthesized beams of FWHM = 0.97″ × 0.94″ and P.A. = 29° for the (2, 2) line and 0.98″ × 0.95″ and 47° for the (3, 3) line, when the imaging was done with a natural weighting. The 1.3 cm continuum data produced a synthesized beam of 1.02″ × 0.91″ and 71°, with a robust weighting.

3. RESULTS AND DISCUSSION

Figure 1 shows the NH_3 (3, 3) line image with an angular resolution similar to the SiO outflow image of Choi (2005). While the NH_3 map shows clumpy structures around the outflows, the most striking feature is the compact structure associated with the central objects, which were not seen in the SiO map. (The outflows will be discussed separately in a future paper.) Figure 2 compares the NH_3 maps with the 1.3 cm continuum map, Table 1 lists the continuum parameters, and Figure 3 shows the

[1]International Center for Astrophysics, Korea Astronomy and Space Science Institute, Hwaam 61-1, Yuseong, Daejeon 305-348, South Korea; minho@kasi.re.kr.

[2]National Astronomical Observatory of Japan, 2-21-1 Osawa, Mitaka, Tokyo 181-8588, Japan.

[3]Department of Astronomy and Space Science, Chungnam National University, Yuseong, Daejeon 305-764, South Korea.

[4] The NRAO is a facility of the National Science Foundation operated under cooperative agreement by Associated Universities, Inc.

[5]See http://aips2.nrao.edu/vla/calflux.html.

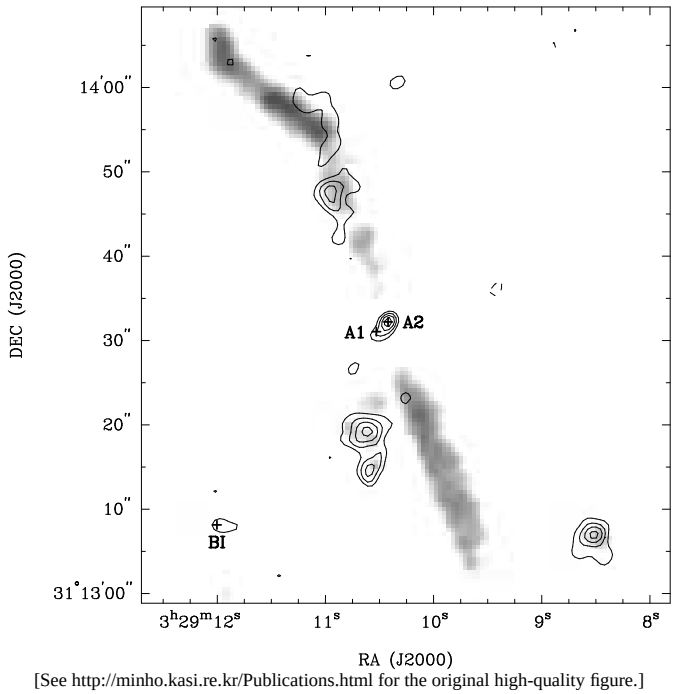

[See http://minho.kasi.re.kr/Publications.html for the original high-quality figure.]

Fig. 1.— Maps of the NH_3 (3, 3) line (*contours*) and the SiO v = 0 J = 1 → 0 line (*gray scale*) toward the NGC 1333 IRAS 4A region. The NH_3 line intensity was averaged over the velocity intervals of $V_{\rm LSR}$ = (–1.0, 14.4) km s^{-1}, which includes the line core and wings. The NH_3 map was convolved to have an angular resolution of FWHM = 2.0″, and the rms noise is 0.20 mJy beam^{-1}. The contour levels are 0.7, 1.0, 1.3, and 1.6 mJy beam^{-1}. Dashed contours are for negative levels. The SiO map is the same as the one shown in Fig. 3*a* of Choi (2005). *Plus signs*: 3.6 cm continuum sources (Reipurth et al. 2002).

NH_3 spectra. The deconvolved FWHM sizes of the NH_3 (3, 3) sources are 350 × 260 AU^2 (1.1″ × 0.8″) for A1 and 260 × 60 AU^2 (0.8″ × 0.2″) for A2, assuming a distance of 320 pc (de Zeeuw et al. 1999). Their compact nature suggests that the NH_3 lines are tracing accretion disks. This interpretation is especially strong in the case of A2 because the emission structure is elongated in the direction perpendicular to the main bipolar outflow. The position angle difference between the minor axis of the A2 disk and the outflow axis is ∼20°. In addition, the blue/redshifted emission peaks of A2 are displaced in a way suggestive of a rotating disk (Fig. 2*c*).

3.1. Flux Anti-correlation

Comparisons of the NH_3 and the continuum maps reveal a remarkable anti-correlation: A1 is brighter than A2 in the continuum map, but it is in the other way around in the NH_3 maps. For a quantitative analysis, we may define an NH_3-to-dust flux ratio $R = F(\mathrm{NH_3})/F(2.7\ \mathrm{mm})$, which is the ratio of the total flux densities of the NH_3 (3, 3) line to the 2.7 mm continuum. The flux densities from the NH_3 data shown in Figure 2*b* and the 2.7 mm data of Looney et al. (2000) give R(A1) = (7.1 ± 1.1) × 10^{-3} and R(A2) = (4.8 ± 0.7) × 10^{-2}. (The uncertainties were estimated by assuming a 10% uncertainty in flux scales.) That is, the NH_3-to-dust flux ratio of A2 is larger than that of A1 by a factor of 6.8 ± 1.4. (If we use the 1.3 cm flux densities, R(A2)/R(A1) is about 12.) Before making interpretations of the flux ratio as column density ratio, several factors affecting the flux densities should be considered.

First, can the line optical depth affect the flux ratio? Since the satellite hyperfine components were not covered in our observations, the optical depth cannot be deduced directly. The line profiles (Fig. 3), however, provide useful information. The spectra toward A2 have larger line widths and higher intensities than those of A1, which suggests that A2 may have relatively larger optical depths. In addition, the (2, 2) spectrum toward A2 shows a self-absorption dip, suggesting that the line may be optically thick. Therefore, if the line optical depth effects are considered, the degree of the anti-correlation would be severer.

Note that, however, there are alternative explanations for the line profiles. The line width difference can be explained if source A2 is a nearly edge-on disk and A1 is either a relatively more face-on disk or a static core. Also, the central dip of the spectra can be caused by a missing flux problem owing to large-scale structures. This issue can be addressed by future observations either with a higher angular resolution or with a spectral coverage wide enough to include the satellite hyperfine components.

Second, can the high NH_3 flux of A2 be caused by a peculiar excitation? The ratio between the (3, 3) and the (2, 2) lines is not very useful for a quantitative analysis because they belong to different species, ortho-NH_3 and para-NH_3, respectively (Ho & Townes 1983). Even so, the (3, 3) to (2, 2) line ratio is similar in both sources (Fig. 3), suggesting that they have similar excitation conditions. In fact, the critical density of the NH_3 inversion transitions are low (∼2 × 10^3 cm^{-3}; Ho & Townes 1983), and the NH_3 molecules are expected to be thermalized. Therefore, it is unlikely that the difference in the NH_3-to-dust flux ratio is caused by a peculiar excitation condition of NH_3 in one of the sources.

Finally, can the dust properties affect the flux ratio? The spectral index in principle provides some information on the dust opacity index. The spectral index of A1 is slightly lower than that of A2 (Table 1), but these values cannot be used directly because the contributions from free-free emission to the 1.3 cm fluxes are not known. Flux measurements at submillimeter wavelengths are desirable for estimating the dust opacity index. Girart et al. (2006) presented a 345 GHz map that resolves the continuum peaks, but their beam size was not quite small enough for measuring the total flux densities of each source separately. Therefore, this issue cannot be resolved with the currently available data, and we presume that the dust opacity index of the two sources are similar. Another variable that can affect the flux ratio is the dust optical depth. The dust is most likely optically thin at centimeter wavelengths, but it could be optically thick at submillimeter. While the measurement of the optical depth is not easy, if this effect is significant, it would affect the stronger source, A1, more severely. Therefore, a correction for the dust optical depth, if necessary, would also make the degree of the anti-correlation severer.

In summary, the results of our observations suggest that the IRAS 4A system contains two sources of contrasting conditions. The NH_3-to-dust flux ratio of A2 is ∼7 times larger than that of A1, and the NH_3-to-dust column density ratios may be different by a similar factor, or by a larger factor if the optical depth of the line or the dust emission is considered. The difference between the two sources is huge, considering that they are accreting matter from a common protostellar envelope, and must be caused by the physical and chemical processes happening in each component.

3.2. Possible Explanations

There are two possible explanations for the flux/column-density anti-correlation of the IRAS 4A system. The main dif-

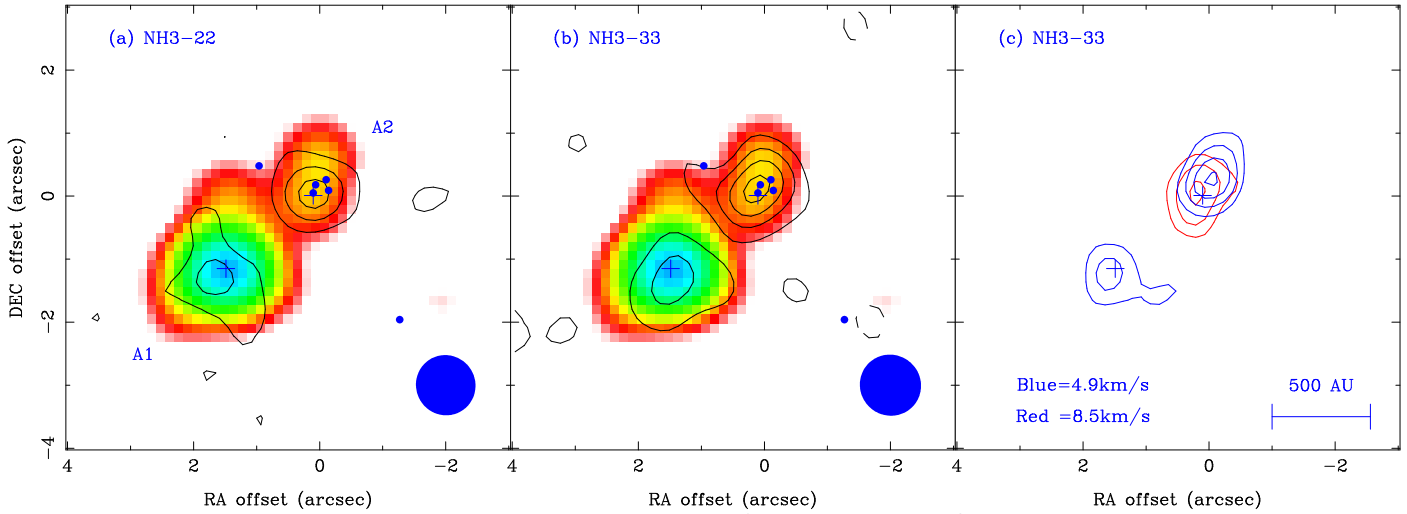

[See http://minho.kasi.re.kr/Publications.html for the original high-quality figure.]

Fig. 2.— Maps of the NH_3 lines (*contours*) and the 1.3 cm continuum (*color scale*). The color scale starts from 0.036 mJy beam^{-1}. Shown at the bottom right corner are the synthesized beams. *Plus signs*: 3.6 cm continuum sources (Reipurth et al. 2002). *Filled circles*: H_2O maser spots (Park & Choi 2007). (*a*) Map of the NH_3 (2, 2) line core. The line intensity was averaged over the velocity interval of V_{LSR} = (4.5, 8.9) km s^{-1}. The contour levels are 1, 2, 3, and 4 times 0.8 mJy beam^{-1}, and the rms noise is 0.27 mJy beam^{-1}. Dashed contours are for negative levels. (*b*) Map of the NH_3 (3, 3) line core. Map parameters are the same as (*a*). (*c*) Maps of the blueshifted and the redshifted emission of the NH_3 (3, 3) line, averaged over the velocity intervals of V_{LSR} = (3.9, 5.8) and (7.6, 9.5) km s^{-1}, respectively. The contour levels are 2, 3, 4, and 5 times 0.6 mJy beam^{-1}. The straight line near the bottom right corner corresponds to 500 AU at a distance of 320 pc.

TABLE 1

NGC 1333 IRAS 4 CONTINUUM SOURCE PARAMETERS

SOURCE	PEAK POSITION		FLUX DENSITY[a]		
	$\alpha_{J2000.0}$	$\delta_{J2000.0}$	Peak	Total	α[b]
A1	03 29 10.53	31 13 31.0	1.44 ± 0.01	1.79 ± 0.03	3.3
A2	03 29 10.41	31 13 32.6	0.19 ± 0.01	0.25 ± 0.02	3.7
BI	03 29 12.00	31 13 08.3	0.36 ± 0.01	0.36 ± 0.01	3.7

NOTE.—Units of right ascension are hours, minutes, and seconds, and units of declination are degrees, arcminutes, and arcseconds.

[a] Flux densities at 1.3 cm in mJy, corrected for the primary beam response.

[b] Spectral index between 1.3 cm and 2.7 mm (Looney et al. 2000). The uncertainty in α is 0.1, assuming that the uncertainty in the absolute flux scale is 10 %.

ference between them is the evolutionary status of A1. While A2 is almost certainly a protostar, the nature of A1 is less certain.

(1) A1 and A2 are roughly coeval, the NH_3 lines trace two accretion disks, and the anti-correlation is caused by a peculiar physical/chemical condition in one of them. In this scenario, A2 is a protostar driving the northeast-southwestern outflow, and A1 is another protostar driving the southern outflow. (We will elaborate on this model in § 3.3.)

(2) A1 and A2 are in quite different stages of evolution, the NH_3 maps show a (spherical) dense core (A1) and an accretion disk (A2), and the anti-correlation is an indication of the difference in their nature. In this scenario, A2 is an actively accreting protostar, and A1 is a pre-protostellar object without an outflow activity. The strong millimeter continuum of A1 suggests a high concentration of dust. Nevertheless, the compact structure detected by interferometers suggests that A1 may not be a usual pre-protostellar object, either. Then A1 could be a transitionary object, either a pre-protostellar object on the verge of collapse or a protostar immediately after the onset of collapse.

We prefer the first explanation for several reasons. First, A1 is bright in the centimeter continuum (Reipurth et al. 2002). This free-free emission is a clear sign of outflow activity. Second, comparison of the mass estimates over a range of size scale indicates that A1 has a steep density gradient. [For example, the mass of the IRAS 4A envelope within a diameter of $\sim 9''$ is 3.2 $M_\odot$, when scaled to the distance of 320 pc (Sandell & Knee 2001). The mass of A1 within a $\sim 2.5''$ box is 1.9 $M_\odot$, when scaled to 320 pc and scaled by the flux ratio between A1 and A2 (Looney et al. 2000). Then the density of A1 (average within a diameter of 820 AU) is higher than the density of the envelope (average within 2900 AU) by a factor of 26 ± 4.] Third, in the second scenario, the southern outflow might be driven by an unknown protostellar object, which is unlikely because NGC 1333 IRAS 4 is one of the most extensively observed regions of star formation near the Sun. Therefore, we suppose that both A1 and A2 are protostars. In the following section, we will discuss the implications of our observations based on the first explanation.

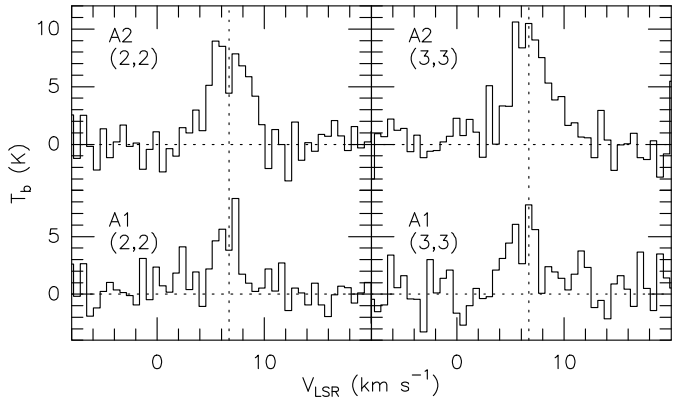

Fig. 3.— Spectra of the NH_3 lines at the peak positions of the 3.6 cm continuum emission (see Fig. 2). Contribution from the dust emission was subtracted by determining the continuum flux level in the velocity intervals of (–6.9, –0.7) and (13.5,19.7) km s^{-1} for the (2, 2) line, and (–9.9, 0.6) and (18.4, 23.3) km s^{-1} for the (3, 3) line. *Vertical dotted lines*: Systemic velocity of the IRAS 4A core ($V_{\rm LSR}$ = 6.7 km s^{-1}; Blake et al. 1995; Choi 2001).

3.3. Peculiarity of the IRAS 4A2 Disk

The difference in the column density ratio suggests that one of the IRAS 4A disks is peculiar. There are several lines of evidence indicating that the A2 disk is unusually active. First, most of the water maser spots in this region are intimately associated with A2 (Fig. 2), and their velocities are close to the systemic velocity of the cloud core (Furuya et al. 2003; Park & Choi 2007), suggesting the existence of shocked gas in the A2 disk. Second, the outflow driven by A2 (northeast-southwestern bipolar outflow) is stronger than the one driven by A1 (southern outflow) (Choi 2005; Choi et al. 2006), also suggesting that the outflow engine (the accretion disk) is more active in A2 than in A1. The northeast-southwestern outflow of IRAS A2 is one of the best collimated molecular outflows (Blake et al. 1995). Third, A2 seems to have an unusually large R value. Comparison with other protostars may tell which disk is the peculiar one. Examples of protostellar disks detected in the NH_3 (3, 3) line is rare, but fortunately IRAS 4BI was detected. IRAS 4BI is a single protostar located within the field of view of our observations (Fig. 1). Measurements of the flux densities give R(BI) = $(4 \pm 2) \times 10^{-3}$, which is similar to R(A1) and suggests that A2 may be the abnormal one. Therefore, the A2 disk may be unusually gas-rich or dust-poor. Such a condition may be possible if the disk is very active or hot so that the dust grains infalling from the protostellar envelope may be destroyed and converted to gaseous molecules, probably via evaporation of molecules in the grain mantle.

The anti-correlation between the gas and the dust flux densities of the IRAS 4A disks has important implications on the star formation process. The standard models of accretion are based on the cases of single central star, and the mass accretion rate is mainly related with the density structure of the protostellar envelope (Shu et al. 1987). In binary systems, however, as the IRAS 4A system shows, even though the two components share a common envelope, each of them can evolve in a distinctive way. That is, there is an important controlling agent that may be lacking in the case of isolated star formation. A possibly crucial factor can be the distribution and (mis-)alignment of angular momentum (Bodenheimer 1995). If the mass outflow rate is a good indicator of the mass accretion rate, A2 may be growing much faster than A1, by accreting matter through an active disk.

One interesting issue to be addressed in the future is the NH_3 abundance. Does the high column-density ratio of A2 mean an overall enhancement of gaseous molecules relative to dust? Or does it mean a selective enhancement of NH_3 (and related species) only? Estimating the degree of enhancement is difficult because comparison with CO lines cannot be interpreted easily owing to the complicated chemistry of nitrogen-bearing molecules (Charnley 1997) and confusion with outflows. Currently there is no reliable estimates of NH_3 abundance in protostellar disks, and it is needed to make high-resolution images of the two disks in a variety of molecular lines.

Since planets do exist in multiple-star systems (Raghavan et al. 2006), our results have interesting implications on the planet formation. If the A2 disk is indeed gas-rich/dust-poor, and if such a condition can persist until the planet-forming phase of the disk evolution, planetary systems produced in such disks may look very different from our solar system. We may speculate that, for example, such a system may strongly favor the growth of gas-giant planets. Thus, multiple-protostar systems can produce diverse types of planetary systems.

We thank J. Cho, K.-T. Kim, and Y. Lee for helpful discussions and encouragement. G. P. was partially supported by the Brain Korea 21 project of the Korean Government.

REFERENCES

Aspin, C., Sandell, G., & Russell, A. P. G. 1994, A&AS, 106, 165
Bachiller, R. 1996, ARA&A, 34, 111
Bally, J., Devine, D., & Reipurth, B. 1996, ApJ, 473, L49
Blake, G. A., Sandell, G., van Dishoeck, E. F., Groesbeck, T. D., Mundy, L. G., & Aspin, C. 1995,
Bodenheimer, P. 1995, ARA&A, 33, 199
Cabrit, S., & André, P. 1991, ApJ, 379, L25
Charnley, S. B. 1997, MNRAS, 291, 455
Choi, M. 2001, ApJ, 553, 219
Choi, M. 2005, ApJ, 630, 976
Choi, M., Hodapp, K. W., Hayashi, M., Motohara, K., Pak, S., & Pyo, T.-S. 2006, ApJ, 646, 1050
de Zeeuw, P. T., Hoogerwerf, R., de Bruijne, J. H. J., Brown, A. G. A., & Blaauw, A. 1999, AJ, 117, 354
Furuya, R. S., Kitamura, Y., Wootten, A., Claussen, M. J., & Kawabe, R. 2003, ApJS, 144, 71
Girart, J. M., Crutcher, R. M., & Rao, R. 1999, ApJ, 525, L109
Girart, J. M., Rao, R., & Marrone, D. P. 2006, Science, 313, 812
Ho, P. T. P., & Townes, C. H. 1983, ARA&A, 21, 239
Lay, O. P., Carlstrom, J. E., & Hills, R. E. 1995, ApJ, 452, L73
Looney, L. W., Mundy, L. G., & Welch, W. J. 2000, ApJ, 529, 477
Park, G., & Choi, M. 2007, ApJ, 664, L99
Raghavan, D., Henry, T. J., Mason, B. D., Subasavage, J. P., Jao, W.-C., Beaulieu, T. D., & Hambly, N. C. 2006, ApJ, 646, 523
Reipurth, B., Rodríguez, L. F., Anglada, G., & Bally, J. 2002, AJ, 124, 1045
Rodríguez, L. F., Anglada, G., & Curiel, S. 1999, ApJS, 125, 427
Sandell, G., Aspin, C., Duncan, W. D., Russell, A. P. G., & Robson, E. I. 1991, ApJ, 376, L17
Sandell, G., & Knee, L. B. G. 2001, ApJ, 546, L49
Shu, F. H., Adams, F. C., & Lizano, S. 1987, ARA&A, 25, 23